JACS
JOURNAL OF THE AMERICAN CHEMICAL SOCIETY

Communication

Uncoordinated amine groups of MOFs to anchor single Ru sites as chemoselective catalysts towards the hydrogenation of quinoline

Xin Wang, Wenxing Chen, Lei Zhang, Tao Yao, Wei Liu, Yue Lin, Huanxin Ju, Juncai Dong, Lirong Zheng, Wensheng Yan, Xusheng Zheng, Zhijun Li, Xiaoqian Wang, Jian Yang, Dongsheng He, Yu Wang, Zhaoxiang Deng, Yuen Wu, and Yadong Li

J. Am. Chem. Soc., **Just Accepted Manuscript** • DOI: 10.1021/jacs.7b01686 • Publication Date (Web): 29 Jun 2017

ACS Publications

Journal of the American Chemical Society is published by the American Chemical Society. 1155 Sixteenth Street N.W., Washington, DC 20036

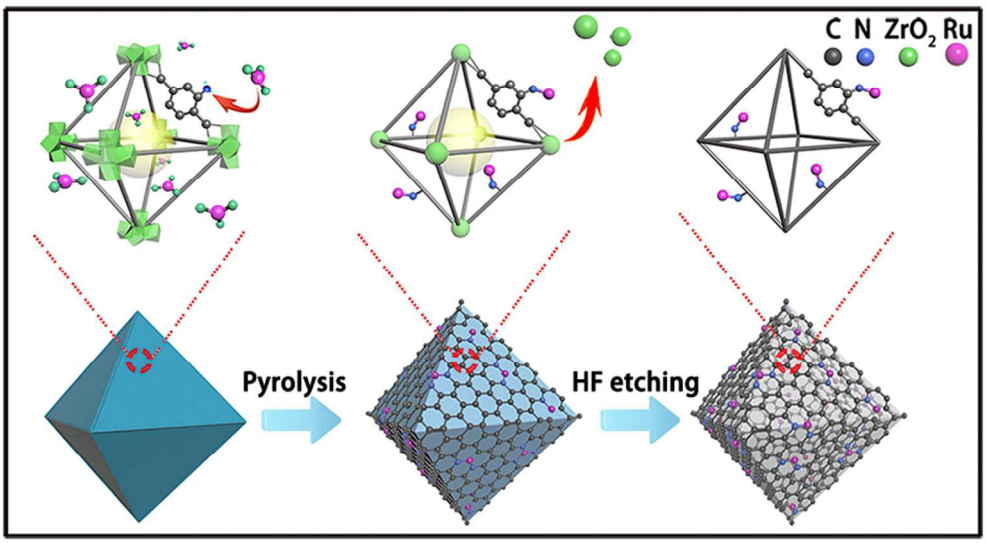

Table of contents

81x44mm (300 x 300 DPI)

Uncoordinated amine groups of MOFs to anchor single Ru sites as chemoselective catalysts towards the hydrogenation of quinoline

Xin Wang,[†,Δ] Wenxing Chen,[‡,Δ] Lei Zhang,[†] Tao Yao,[§] Wei Liu,[§] Yue Lin,[†] Huanxin Ju,[§] Juncai Dong,[⊥] Lirong Zheng,[⊥] Wensheng Yan,[§] Xusheng Zheng,[§] Zhijun Li,[†] Xiaoqian Wang,[†] Jian Yang,[†] Dongsheng He, [†] Yu Wang,[#] Zhaoxiang Deng,[†] Yuen Wu,*[,†] and Yadong Li*[,‡]

[†]Department of Chemistry, iChEM (Collaborative Innovation Center of Chemistry for Energy Materials), University of Science and Technology of China, Hefei 230026, China

‡ Department of Chemistry, Tsinghua University, Beijing 100084, China

[§] National Synchrotron Radiation Laboratory (NSRL), University of Science and Technology of China, Hefei, Anhui 230029, China

[⊥]Institute of High Energy Physics Beijing 100029 (China)

#Shanghai Synchrontron Radiation Facilities, Shanghai Institute of Applied Physics, Chinese Academy of Science, Shanghai 201800, China

Supporting Information Placeholder

ABSTRACT: Here we report a precise control of isolated single ruthenium site supported on nitrogen-doped porous carbon (Ru SAs/N-C) through a coordination-assisted strategy. This synthesis is based on the utilization of strong coordination between Ru^{3+} and the free amine groups (-NH_2) at the skeleton of metal-organic framework (MOF), which plays a critical role to access the atomically isolated dispersion of Ru sites. Without the assistance of the amino groups, the Ru precursor is prone to aggregation during the pyrolysis process, resulting in the formation of Ru clusters. The atomic dispersion of Ru on N-doped carbon can be verified by the spherical aberration correction electron microscopy and x-ray absorption fine structure (XAFS) measurements. Most importantly, this single Ru sites with single-mind N coordination can serve as a semi-homogeneous catalyst to effectively catalyze chemoselective hydrogenation of functionalized quinolones.

Considering the global motif of sustainable development in energy and environment area, isolated single site catalysts have attracted extensive attention due to their maximum atom utilization and superior reactivity and selectivity.[1] As an ideal model bridging between heterogeneous and homogeneous catalysis, the performance of catalysts based on single atoms is highly related to their structures, such as coordination ligands, dispersion gesture and interactions with supports.[2] To date, traditional synthetic protocol to access single atom catalysts are commonly based on an initial adsorption of metal precursor with a subsequent reduction process. Therefore, the final properties of single site catalysts are highly dependent upon the binding and stabilization of support. The design of the anchoring sites, which are usually the oxygen or carbon vacancies, is the key to achieve the atomic dispersion and identical geometric structure for homogenized catalytic sites.[3-5] Therefore, developing rational and general synthetic methods to construct well-defined single sites catalysts, that can potentially/ideally inherit the merits of homogeneous and heterogeneous analogues, are highly desired but challenging.

Although abundant works employing MOFs as precursors to access the metal/MOFs hybrids have been reported, few of them focused on the preparation of single metal atoms catalysts.[6-7] Recently, our group reported that single atom catalysts can be prepared by converting atomically dispersed metal nodes *in-situ* from MOFs.[8] However, noble metals (Au, Ag, Pt, Ru ions, etc.) have been rarely used as the nodes of MOFs, thus hindering the *in-situ* evolution from metal nodes to single atoms catalysts.[9-10] Ru-based nanomaterials have proven to be effective in various catalytic reactions.[11] Herein, we have utilized the uncoordinated -NH_2 located at the terephthalic acid linkers in UiO-66-NH_2 as the Lewis base to stabilize the $RuCl_3$. The strong interaction between lone pair electrons and d-orbitals would ensure the Ru single atoms to be confined in the pores of MOFs and prevent their aggregation during the pyrolysis at high temperature. Without the assistance of free -NH_2, Ru clusters were found to be the dominant moieties dispersing on the final porous carbon. These differently gathered Ru catalysts exhibit size-dependent catalytic properties towards the hydrogenation of quinolones, revealing a robust route to tailor and optimize the activity and selectivity by atomic-scale design.

The MOFs chosen for hosting the Ru atoms was UiO-66, $[Zr_6O_4(OH)_4(BDC)_6$ (BDC=1,4-benzenedicarboxylate)], which features three-dimensional structure, uniform porosity, high surface area, and robust thermal and chemical stability.[12] The derivative UiO-66-NH_2, during which the BDC was functionalized with ammonium, could largely inherit the symmetry and morphology of UiO-66 (Figure S1).[13] Merging $ZrCl_4$ and BDC with the $RuCl_3$ during the synthesis process, the Ru ions were adsorbed within the evacuated UiO-66 or UiO-66-NH_2 to obtain the corresponding complexes. As shown in Figure S2, these adsorption processes do not change the octahedral shape of inital polyhedrons and size distribution. The powder X-ray diffraction (XRD) pattern of the sample collected after the adsorption of $RuCl_3$ displayed characteristic peaks of UiO-66, demonstrating the retention of UiO-66 crystallinity and structure (Figure S3). The interaction of $RuCl_3$ precursors with the -NH_2 groups of UiO-66-NH_2 was further confirmed by FT-IR spectroscopy. The peaks at 1620 and 1060 cm^{-1} (Figure S4) can be ascribed to the -NH_2 scissoring and rocking vibrations, respectively.[14] The intensity changes and position shifts of the peaks strongly support the interaction between Ru ions and -NH_2 groups. Following a pyrolysis process at 700 °C, the building skeleton of UiO-66 was transferred *in-situ* into porous carbon, which was decorated by small ZrO_2 crystals and Ru species. As revealed by the XRD pattern in Figure S3c, the addition of HF solution could readily etch the inert ZrO_2 nanoparticles, resulting in the formation of Ru single atoms (0.30 wt% Ru loading) or Ru clusters (0.35 wt% Ru loading) within the carbon architecture (Ru SAs/N-C or Ru NCs/C).

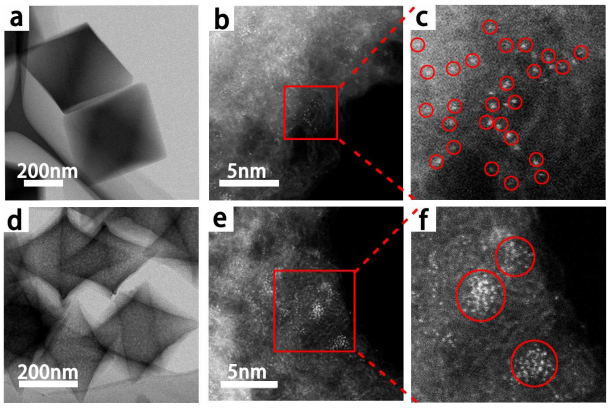

Figure 1. (a) TEM of Ru SAs/N-C, (b,c) magnified HAADF-STEM images of Ru SAs/N-C. (d) TEM of Ru NCs/C, (e, f) magnified HAADF-STEM images of Ru NCs/C.

Transmission electron microscopy (TEM) and scanning electron microscope (SEM) images (Figure 1a, d and Figure S5) revealed the as-prepared Ru SAs/N-C and Ru NCs/C structure remained the starting octahedral shape of UiO-66-NH_2 and UiO-66, respectively. The image of aberration corrected high-angle annular dark-field scanning transmission electron microscope (HAADF-STEM) revealed the brighter spots assigned to the heavier Ru atoms exhibited atomic dispersion on the N-doped carbon support (Figure 1b,c). Some Ru single atoms were circled in red for better obseravation (Figure 1 c). This strongly supports that the uncoordinated -NH_2 groups could stabilize the $RuCl_3$ precursor and further prevent their assembling during pyrolysis. By contrast, without the assistance of -NH_2 groups, a large proportion of Ru atoms would aggregate at high temperature, resulting in the formation of clusters on the support (Figure 1e and f).

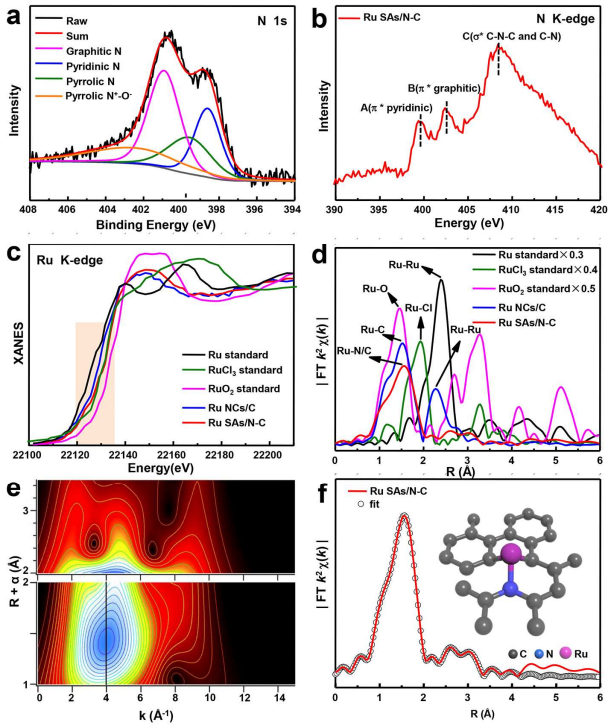

Figure 2. (a) XPS spectra for the N 1s region of Ru SAs/N-C. (b) N K-edge NEXAFS spectra of Ru SAs/N-C. (c) XANES spectra of Ru SAs/N-C and Ru NCs/C for Ru K-edge. (d) Fourier transformed (FT) k^2-weighted $\chi(k)$-function of the EXAFS spectra for Ru K-edge. (e) WT of the Ru-K edge and (f) Fitting results of the EXAFS spectra of Ru SAs/N-C.

The X-ray diffraction (XRD) patterns for the Ru SAs/N-C and Ru NCs/C showed no characteristic peaks of Ru crystals, excluding the generation of large particles and aggregates (Figure S3c). X-ray photoelectron spectroscopy (XPS) was used to characterize the valence state of N (Figure 2a) and C (Figure S6). The peak at 401.3 eV and its shakeup satellites could be assigned to graphitic N. The pyridinic N (398.7 eV) and pyrrolic N (398.7 eV) are dominant in the Ru SAs/NC. These two types of N atoms are located in a π conjugated system,[15] whose p-electrons synergistically facilitated the stabilization of Ru SAs. Studies have shown that N doping in carbon support could effectively introduce a large amount of topological defects, and the corresponding density is related to the I_D/I_G value in Raman spectra.[16] The intensity ratios of I_D/I_G for Ru SAs/N-C and Ru NCs/C are calculated to be 1.01 and 0.97, respectively (Figure S7a). This supports our hypothesis that there would be more dispersive defects in the Ru SA/N-C than Ru NCs/C.[17]

To further investigate the electronic structure of the catalysts, near edge X-ray absorption fine structure (NEXAFS) measurements were performed (Figure 2b and Figure S8a). The observed C K-edge spectra of Ru SAs/N-C and Ru NCs/C are quite similar, suggesting similar environments of carbon skeletons present. The peak A (ca. 285.6 eV) was derived

from C-C π* (ring) excitations, and the peak C (ca. 293.2 eV) was originated from C-C σ* (ring) transitions.[18] The occurrence of both peaks implies a graphitization process during the pyrolysis. Interestingly, sharp peaks at 288.4 eV (peak B) were observed for both Ru SAs/N-C and Ru NCs/C, whereas no peaks associated with flaky graphite powder were found (Figure S8b).[19] Since the peak B was assigned to C-O-C or C-N-C, the above difference indicates that there are a plenty of defect sites in the carbon lattice for Ru SAs/N-C.[20-21] For the N K-edge spectrum (Figure 2b), the peak A (at 399.5 eV) and peak B (at 402.4 eV) result from pyridinic π* and graphitic π* transitions, respectively. The peak C (at 408.5 eV) suggests the formation of C-N-C or C-N σ* bond.

To verify the formation of Ru sub-nano species and explore their inherent structures at atomic level, we performed the XAFS measurements of Ru K-edge. The XANES spectra (Figure 2c and Figure S9a) show that the absorption threshold for the Ru SAs/N-C is close to that of $RuCl_3$, indicating the valence state of Ru is close to 3+ (Figure S9b). The curves for both Ru SAs/N-C and Ru NCs/C have a main peak around 1.5 Å, corresponding to the Ru-N/C scattering pair (Figure 2d). Ru-Cl coordination is absent and no Ru oxide species can be observed. We also notice that there is another coordination peak at 2.25 Å for Ru NCs/C, which can be ascribed to a metallic Ru-Ru scattering peak. This suggests that the Ru present in the form of clusters in Ru NCs/C, consistent with the TEM results (Figure 1e and 1f). In contrast, the metallic Ru-Ru peak for the Ru SAs/N-C is negligible, which supports the hypothesis that almost all the Ru atoms in Ru SAs/N-C are atomically dispersed.[22-23] To further explore the atomic dispersion of Ru in Ru SAs/N-C, wavelet transform (WT) of Ru K-edge EXAFS was carried out.[24] In Figure 2e, the WT contour plots of Ru SAs/N-C show only one intensity maximum at 4.0 $Å^{-1}$, corresponding to Ru-N/C coordination. Additionally, no intensity maximum related to Ru-Ru contribution can be found at high coordination shells, compared with the WT plot of Ru foil in Figure S10. Quantitative EXAFS analyses were performed and the fitting results are shown in Figure 2f, S11, S12 and Table S1. The first shell of the Ru atom in Ru SAs/N-C has a coordination number of three and a mean bond length of 2.08 Å (insert of Figure 2f).

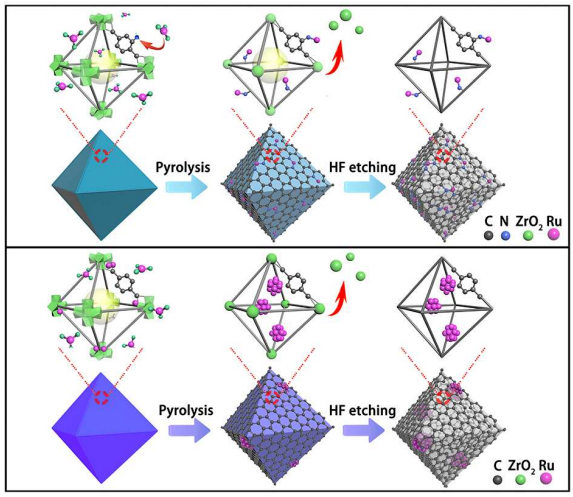

Figure 3. Scheme of the proposed formation mechanisms for Ru SAs/N-C (top) and Ru NCs/C (bottom).

Figure 3 shows the proposed formation mechanism of Ru SA/N-C. Since UiO-66-NH_2 possess abundant dangling -NH_2 groups, Ru metal ions can be adsorbed within the MOFs channels by the strong coordination interaction between the electron lone pair of nitrogen and d-orbital of Ru atoms. After the pyrolysis process, the ligand and Zr-based anodes of UiO-66-NH_2 would form porous C and ZrO_2 nanoparticles, respectively. Meanwhile, the adsorbed Ru ions can be reduced by the surrounding carbon. It is worth pointing out that the dangling -NH_2 played a critical role in the formation of Ru SAs, as they can largely limit the diffusion of Ru atoms at high temperature and bond with adjacent Ru atoms. Without the dangling -NH_2, the Ru ions tended to aggregate into nanoclusters and small nanoparticles at high-temperature even in confined pores of MOFs.

Brunauer-Emmett-Teller (BET) adsorption–desorption isotherms revealed that the Ru SAs/N-C and Ru NCs/C exhibited large pore volume and surface area (Figure S13). This feature contributes to the exposure of active sites and benefits rapid transportation of hydrogenation-relevant substrates. Quinoline hydrogenation involves the regioselective hydrogenation of the nitrogen-containing ring to form the (py-THQ, 1a).[25] However, by-products such as 5,6,7,8- tetrahydroquinoline (bz-THQ, 1b) and decahydroquinoline (DHQ, 1c) may inevitably form during the reaction. For example, commercial Ru/C catalyst has only 9.0% selectivity toward py-THQ.[26]

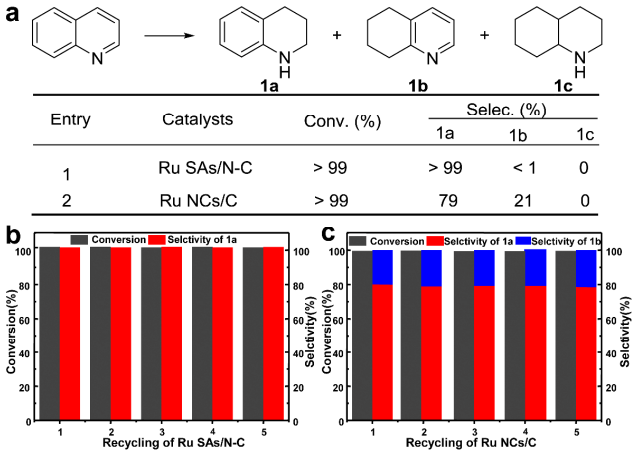

Figure 4. (a) Catalytic performance of Ru SAs/N-C and Ru NCs/C catalysts for the regioselective hydrogenation of quinolin. Catalytic activity and chemoselectivity of (b) Ru SAs/N-C and (c) Ru NCs/C in the hydrogenation of quinoline.

As shown in Figure 4a, quinoline can be converted completely by employing either Ru SAs/N-C or Ru NCs/C, however, the corresponding selectivity for the desired products was observed to be different. The Ru SAs/N-C obtained more than 99% selectivity towards py-THQ (1a), which is much higher than that of Ru NCs/C (79%). It can be inferred the multiple reactive sites on the Ru clusters should be accounted for the diversity of products. Due to the uniform structure of isolated active Ru sites, the Ru SAs/N-C achieved almost exclusive selectivity for py-THQ (1a), while maintaining an excellent conversion efficiency of quinoline (>99%). We further investigated the durability of Ru SAs/N-C and Ru NCs/C toward this hydrogenation reaction. As shown in Figure 4b, the activity and selectivity of Ru SAs/N-

C catalysts were retained after 5 recycles of hydrogenation reactions. TEM images of the Ru SAs/N-C after the durability test revealed that the atomic dispersion of Ru atoms remained unchanged (Figure S14). More interestingly, the Ru SAs were hardly observed for the Ru NCs/C after the durability test, indicating the single atom species was unstable during the catalysis without the protection of free -NH_2 groups. This evolution process was analogous to the well-known Ostwald ripening phenomena.[27] The active single Ru atoms were inclined to bond with the more stable Ru cluster, resulting in the disappearance of single Ru sites. For Ru NCs/C catalyst, the selectivity to py-THQ and its yield nearly did not deteriorate, demonstrating the Ru clusters were dominant reactive sites during the catalytic cycles.

Having established active and selective Ru SAs/NC catalyst, we further studied the hydrogenation of various structural different substituted quinolines. As depicted in Table S2, the hydrogenation of 6- and 8-hydroxyquinolines afforded the corresponding biologically active 1,2,3,4-tetrahydro-6-hydroxyquinolines and 1,2,3,4-tetrahydro-8-hydroxyquinolines (Table S2, entries 1 and 2), respectively. Remarkably, the hydrogenation of quinolines with electron-donating groups $-NH_2$ at the 6- and 8-position on the benzene ring was also highly regioselective (Table S2, entries 3 and 4). In a more challenging reaction, where quinolines bearing other halogens groups, the corresponding valuable functional tetrahydroquinolines were obtained in excellent yield (Table S2, entries 5-7). Moreover, this highly selective Ru SAs/N-C could be also applied to effect the generation of 1,2,3,4-Tetrahydroisoquinoline (Table S2, entry 8). Catalyzed by the Ru NCs/C, diverse products were also detected for the hydrogenation of functional quinolones (Table S3).

In summary, we report the preparation of single Ru sites by employing uncoordinated functional groups on skeletons of MOFs. Our findings opened new opportunities to synthesize single metal atoms anchored on N-doped carbon support for various applications.

ASSOCIATED CONTENT

Supporting Information

Detailed experimental procedures; SEM images; FT-IR spectra; EELS mapping; XRD and XPS spectra. This material is available free of charge via the Internet at http://pubs.acs.org.

AUTHOR INFORMATION

Corresponding Author

yuenwu@ustc.edu.cn; ydli@mail.tsinghua.edu.cn

ACKNOWLEDGMENT

This work was supported by China Ministry of Science and Technology under Contract of 2016YFA (0202801), and the National Natural Science Foundation of China (21522107, 21671180, 21521091, 21390393, U1463202). This work made use of the resources and finance support of National Synchrotron Radiation Laboratory in Beijing and Shanghai.

REFERENCES

(1) Yang, X.-F.; Wang, A.; Qiao, B.; Li, J.; Liu, J.; Zhang, T. *Acc. Chem. Res.* **2013**, *46*, 1740.

(2) Deng, D.; Chen, X.; Yu, L.; Wu, X.; Liu, Q.; Liu, Y.; Yang, H.; Tian, H.; Hu, Y.; Du, P. *Sci. Adv.* **2015**, *1*, e1500462.

(3) Schaub, R.; Wahlström, E.; Rønnau, A.; Lægsgaard, E.; Stensgaard, I.; Besenbacher, F. *Science* **2003**, *299*, 377.

(4) Zhou, C.; Kong, J.; Yenilmez, E.; Dai, H. *Science* **2000**, *290*, 1552.

(5) Maciel, I. O.; Anderson, N.; Pimenta, M. A.; Hartschuh, A.; Qian, H.; Terrones, M.; Terrones, H.; Campos-Delgado, J.; Rao, A. M.; Novotny, L. *Nat. Mater.* **2008**, *7*, 878.

(6) Lu, G.; Li, S.; Guo, Z.; Farha, O. K.; Hauser, B. G.; Qi, X.; Wang, Y.; Wang, X.; Han, S.; Liu, X. *Nat. Chem.* **2012**, *4*, 310.

(7) Cao, X.; Tan, C.; Sindoro, M.; Zhang, H. *Chem. Soc. Rev.* **2017**. DOI:10.1039/C6CS00426A

(8) Yin, P.; Yao, T.; Wu, Y.; Zheng, L.; Lin, Y.; Liu, W.; Ju, H.; Zhu, J.; Hong, X.; Deng, Z.; Zhou, G.; Wei, S.; Li, Y. *Angew. Chem. Int. Ed.* **2016**, 55, 10800.

(9) Lee, J.; Farha, O. K.; Roberts, J.; Scheidt, K. A.; Nguyen, S. T.; Hupp, J. T. *Chem. Soc. Rev.* **2009**, *38*, 1450.

(10) Zhou, H.-C.; Long, J. R.; Yaghi, O. M. *Chem. Rev.* **2012**, *112*, 673.

(11) Chen, G.; Zhang, J.; Gupta, A.; Rosei, F.; Ma, D. *New J. Chem.* **2014**, *38*, 1827.

(12) Cavka, J. H.; Jakobsen, S.; Olsbye, U.; Guillou, N.; Lamberti, C.; Bordiga, S.; Lillerud, K. P. *J. Am. Chem. Soc.* **2008**, *130*, 13850.

(13) Kandiah, M.; Nilsen, M. H.; Usseglio, S.; Jakobsen, S.; Olsbye, U.; Tilset, M.; Larabi, C.; Quadrelli, E. A.; Bonino, F.; Lillerud, K. P. *Chem. Mater.* **2010**, *22*, 6632.

(14) Karabacak, M.; Cinar, M.; Unal, Z.; Kurt, M. *J. Mol. Struct.* **2010**, *982*, 22.

(15) Casanovas, J.; Ricart, J. M.; Rubio, J.; Illas, F.; Jiménez-Mateos, J. M. *J. Am. Chem. Soc.* **1996**, *118*, 8071.

(16) Suenaga, K.; Yudasaka, M.; Colliex, C.; Iijima, S. *Chem. Phys. Lett.* **2000**, *316*, 365.

(17) Wei, D.; Liu, Y.; Wang, Y.; Zhang, H.; Huang, L.; Yu, G. *Nano Lett.* **2009**, *9*, 1752.

(18) Zhang, L. S.; Liang, X. Q.; Song, W. G.; Wu, Z. Y. *Phys. Chem. Chem. Phys.* **2010**, *12*, 12055.

(19) Skytt, P.; Glans, P.; Mancini, D. C.; Guo, J. H.; Wassdahl, N.; Nordgren, J.; Ma, Y. *Phys. Rev. B* **1994**, 50, 10457.

(20) Liang, Y.; Li, Y.; Wang, H.; Zhou, J.; Wang, J.; Regier, T.; Dai, H. *Nat. Mater.* **2011**, *10*, 780.

(21) She, X.; Wu, J.; Zhong, J.; Xu, H.; Yang, Y.; Vajtai, R.; Lou, J.; Liu, Y.; Du, D.; Li, H.; Ajayan, P. M. *Nano Energy* **2016**, *27*, 138.

(22) Maschmeyer, T.; Rey, F.; Sankar, G.; Thomas, J. M. *Nature* **1995**, *378*, 159.

(23) Liu, P.; Zhao, Y.; Qin, R.; Mo, S.; Chen, G.; Gu, L.; Chevrier, D. M.; Zhang, P.; Guo, Q.; Zang, D. *Science* **2016**, 352, 797.

(24) Fei, H.; Dong, J.; Arellano-Jimenez, M. J.; Ye, G.; Dong Kim, N.; Samuel, E. L.; Peng, Z.; Zhu, Z.; Qin, F.; Bao, J.; Yacaman, M. J.; Ajayan, P. M.; Chen, D.; Tour, J. M. *Nat. Commun.* **2015**, *6*, 8668.

(25) Chen, F.; Surkus, A. E.; He, L.; Pohl, M. M.; Radnik, J.; Topf, C.; Junge, K.; Beller, M. *J. Am. Chem. Soc.* **2015**, *137*, 11718.

(26) Chen, Y.; Yu, Z.; Chen, Z.; Shen, R.; Wang, Y.; Cao, X.; Peng, Q.; Li, Y. *Nano Res.* **2016**, *9*, 2632.

(27) Talapin, D. V.; Rogach, A. L.; Haase, M.; Weller, H. *J. Phys. Chem. B.* **2001**, *105*, 12278.